Effect of Nanoconfinement on the isodimorphic crystallization of Poly(butylene succinate-ran-caprolactone) Random Copolymers

Maryam Safari[1], Laia Leon Boigues[2], Guangyu Shi[3,4], Jon Maiz[1], Guoming Liu*[3,4], Dujin Wang[3,4], Carmen Mijangos*[2,5], Alejandro J. Müller*[1,6]

[1]*POLYMAT and Polymer Science and Technology Department, Faculty of Chemistry, University of the Basque Country UPV/EHU, Paseo Manuel de Lardizábal, 3, 20018 Donostia-San Sebastián, Spain.*

[2]*Instituto de Ciencia y Tecnología de Polímeros, Consejo Superior de Investigaciones Científicas, ICTP-CSIC, Juan de la Cierva 3, Madrid 28006, Spain.*

[3]*Beijing National Laboratory for Molecular Sciences, CAS Key Laboratory of Engineering Plastics, CAS Research/Education Center for Excellence in Molecular Sciences, Institute of Chemistry, the Chinese Academy of Sciences, Beijing 100190, China.*

[4]*University of Chinese Academy of Sciences, Beijing 100049, China.*

[5]*Departamento de Física de Materiales, University of the Basque Country UPV/EHU and Centro de Física de Materiales (CFM) (CSIC-UPV/EHU) - Materials Physics Center (MPC), Paseo Manuel de Lardizabal 5, 20018 San Sebastián, Spain.*

[6]*IKERBASQUE, Basque Foundation for Science, Bilbao, Spain.*

**Corresponding authors: gmliu@iccas.ac.cn; cmijangos@ictp.csic.es; alejandrojesus.muller@ehu.es*

TOC graphic

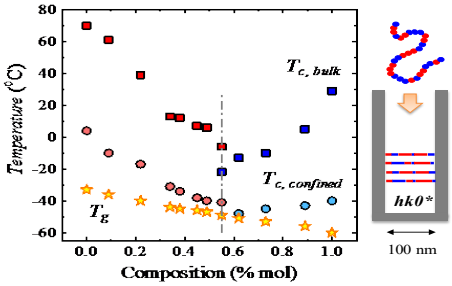
Temperature (°C)
Composition (% mol)
$T_{c,\ bulk}$
$T_{c,\ confined}$
T_g
hk0*
100 nm

ABSTRACT

In this paper, we study for the first time the effect of hard confinement on the isodimorphic crystallization of random copolyesters. A series of poly(butylene succinate-*ran*-caprolactone) samples encompassing the entire composition range were successfully infiltrated into nanoporous alumina templates (AAO) with a fixed diameter of 100 nm. Samples were characterized using scanning electron microscopy (SEM), Raman spectroscopy, Fourier transform infrared spectroscopy (FTIR), differential scanning calorimetry (DSC) and grazing-incidence wide-angle X-ray diffraction (GIWAXS). FTIR proved that PBS-rich nanofibers showed interactions between the copolyester chains and the walls of the AAO templates; however, the PCL-rich nanofibers did not show any interaction with the AAO walls. All infiltrated samples experienced a very large decrease in crystallization temperature, as expected, since the level of confinement is large enough to suppress heterogeneous nucleation. In spite of this, all copolymers were able to crystallize, regardless of composition. Additionally, when T_c or T_m are plotted versus copolymer composition a clear pseudo-eutectic point is observed. These results indicate that the isodimorphic behavior of the copolyesters is maintained under hard confinement. Infiltrated PCL undergoes homogeneous nucleation (inside the nanopore volume) as expected by the lack of interaction with the AAO walls. On the other hand, PBS exhibited a surface nucleation mechanism triggered by the interactions with the AAO walls. In the case of random copolymers, all PCL-rich copolymers nucleated homogeneously. However, in the case of PBS-rich copolymers, the nucleation gradually changed from surface-induced nucleation for neat PBS to homogeneous nucleation, as PCL concentration in the copolymers increased and the interactions of PBS chains with the AAO walls are diluted. The confinement under 100 nm nanopores did not change the orientation of the PBS or PCL phase crystals, which kept their chain direction perpendicular to the pore axis, as demonstrated by GIWAXS.

Keywords: *biocopolyesters; confinement; isodimorphism; homogeneous nucleation; crystallization.*

INTRODUCTION

One-dimensional (1D) polymers are an interesting area in the nanotechnology field[1-3]. A number of nano-molding techniques have been established to prepare 1D nanostructures. Among them, one of the most successful, low-cost and fast-manufacturing methods is polymer infiltration into inorganic templates. Anodic aluminum oxide (AAO) templates have become a research hotspot because of their advantages of inexpensive, high thermal and mechanical stability, and promising potential for scalable production[4-10]. Polymer infiltration within AAO nanoporous templates is an excellent strategy for nano-patterning[3,11].

The interest in employing semi-crystalline polymers in nanotechnology applications has been growing over the last few decades[4,12-23]. The main interest of confining semi-crystalline polymers is to create very small and isolated microdomains, which can be easily achieved by employing porous AAO templates. Many works have shown that polymer confinement contributes to many unique features of their structure and properties[18,24-30]. In terms of semi-crystalline polymers, confinement contributes to a drastic depression in crystallization temperature[18,20,25], a drop in crystallinity[24,31], preferential orientation of crystals[20,25,29,32-34], changes in crystallization kinetics[35-37], polymorphism and crystal transitions[33,37-42]. To date, great advances have been achieved on the understanding of the crystallization behavior of homopolymers under confinement; however, the study of random copolymers under confinement is still rare.

Random biodegradable copolymers have been recently studied for their unique crystallization behavior[43]. Multiple features can be found in random copolymers with two crystallizable components. Two crystal structures can be formed in isodimorphic random

copolyesters depending on their composition. The thermal properties indicate a pseudo-eutectic region, in which the two components of the copolymer have the same chance to crystallize. The fact is that this kind of copolymers crystallizes over the whole composition range, making their properties tunable just by changing the composition or even the thermal history of such copolyesters (e.g., changing the thermal history at the pseudo-eutectic point)[44-49].

Several examples of isodimorphic and isomorphic copolyesters were reported and discussed in the recent reviews of Pérez *et al*.[50] and Pan *et al*.[51]. Most of them are based on polyesters and poly(hydroxialcanoates), such as P(HS-*ran*-HA)[52], P(BS-*ran*-HS)[53], P(BS-*ran*-BAz)[54], P(BS-*ran*-BA)[45], P(BL-*ran*-CL)[55], P(CL-*ran*-DL)[56]. In our previous works[57,58], we have synthesized high M_w PBS-*ran*-PCL copolyesters and studied their morphological and thermal characterization in detail. We found that these random copolyesters show an isodimorphic behavior. It means that the morphology and properties of these copolyesters can be tailored by varying their composition, molecular weight or even their thermal history [50,58].

We have previously shown that at the pseudo-eutectic point, two crystalline phases are usually form, while compositions away from the pseudo-eutectic form a single crystalline phase. This double crystallization at the pseudo-eutectic compositions strongly depends on cooling rates or isothermal crystallization temperature[45,57,58]. Since the confinement provides a well-defined way of controlling the crystallization kinetics, it is interesting to investigate how the isodimorphic crystallization behavior changes under confinement. In this work, we studied, for the first time, the isodimorphic crystallization behavior of poly(butylene succinate-*ran*-caprolactone) random copolymers under confinement within nanoporous alumina templates (AAO). The infiltration of the polymer was studied by Raman spectroscopy and SEM. FTIR was applied to study the interaction between the polymer and the AAO walls. The crystallization and

melting behavior were studied by DSC. The morphology and crystalline structure was studied by SEM, and GIWAXS.

EXPERIMENTAL

Materials and methods

Synthesis of PBS-*ran*-PCL copolyesters. The PBS-*ran*-PCL copolyesters used in this study, were synthesized by a two-stage melt-copolymerization reaction that is described in our previous work in full detail[58]. In brief, we have done transesterification/ROP reactions of dimethyl succinate (DMS), 1,4-butanediol (BD), and ε-caprolactone (CL) at 160 ºC under nitrogen flow. Polycondensation reactions were completed at 190 ºC and under vacuum. The copolyesters are denoted in an abbreviated form, BS_xCL_y, subscripts x and y indicating the molar ratio of each component that were determined by ^{1}H NMR. Table SI-1 shows molar composition of each copolyester, number-average molecular weight and glass transition temperature (extracted from non-isothermal DSC measurements) of the isodimorphic random copolyesters under this study.

Manufacturing the nanostructures (nano-molding) using AAO templates. The infiltration of PBS-*ran*-PCL copolymers was performed applying the melt-wetting technique under vacuum. The AAO templates with a diameter of 100 nm were purchased from Shanghai Shangmu Technology Co. Ltd. Polymer films made from copolyesters were placed on top of the AAO template surface and then infiltrated by heating them to 40 °C above the corresponding melting point of each copolyester under nitrogen flow. After the melt-infiltration process for 12h, the samples were cleaned in order to eliminate any polymeric residue from the AAO surface in four steps, as follows: 1. Removing the residue bulk polymer from the top surface of the template

using a sharp blade at ambient temperature, 2. Then, samples were gently cleaned with a gauze at a temperature above the corresponding melting temperature of the copolymer, 3. In this step, the sample's surface was softly polished using sandpaper (180 grit), 4. To complete the cleaning process, the top surface of the templates was wiped off with chloroform.

Characterization Methods

Scanning Electron Microscopy (SEM). A Philips XL-30 ESEM microscope was used to characterize the morphology of the obtained polyester nanofibers. To observe the polymeric nanofibers inside the AAO templates by SEM, the templates filled with copolymer were fractured in liquid nitrogen.

Raman and Fourier Transformed Infrared (FTIR) Spectroscopies. A Raman Microscope (Renishaw plc, Wottonunder-Edge, UK) attached to a confocal microscope and fitted with a Peltier-cooled charge-coupled device (CCD) detector and a spectrometer of 785 nm near-infrared diode laser was employed. All spectra were analyzed by Renishaw WiRE software. The spectral range was between 4000−500 cm^{-1} with 4 cm^{-1} spectral resolution. To study the polymeric nanofibers after the infiltration process, samples were studied by FTIR using a PerkinElmer Spectrum One with an attenuated total reflectance (ATR) attachment.

Characterization of the Crystalline Structure

Crystallization Protocol. Differential scanning calorimetry (DSC) helped us to examine the non-isothermal crystallization behavior of both bulk and infiltrated polymers using a DSC-Q2000, TA calorimeter under a nitrogen atmosphere flow calibrated with Indium. Approximately 5 mg of bulk polyester or 20 mg of confined polyester inside AAO were placed and sealed well in standard aluminum pans. First, samples were held at 30 °C above their

corresponding melting point for 3 min to erase thermal history. Then, the samples were cooled down to -100 °C at 10 °C/min and held at -100 ºC for 1 min. Subsequently, they were heated up to 30 ºC above their corresponding melting points. All infiltrated copolyester samples were measured inside the AAO template with its aluminum base. In this paper, we use the exothermic and endothermic peaks, corresponding to the first order transitions determined by non-isothermal DSC, as the characteristic crystallization (T_c) and melting (T_m) temperatures of the samples.

To determine the glass transition temperature (T_g), samples were heated up to 30 °C above their melting point. Then, they were quenched to -90 °C at a cooling rate of approximately 160 ºC/min. Finally, the DSC heating scan was recorded at 20 °C/min. The T_g values were extracted from the midpoint of the jump in heat capacity.

X-Ray Scattering. Grazing incidence wide-angle X-ray scattering (GIWAXS) patterns were measured with a Xeuss 2.0 WAXS/SAXS system (Xenocs SA, France). The instrument was equipped with a Cu K_α source and a two-dimensional detector (Pilatus 300K, DECTRIS, Swiss). The wavelength of the X-ray radiation was 1.5418 Å. The X-ray beam was incident on the AAO surface with a ~3° angle. The exposure time was 20 min for the infiltrated samples and 5 min for the bulk sample. Intensity profiles were obtained by averaging the 2D patterns. All samples shared the same thermal history: (I) erasing thermal history at 30 °C above their corresponding melting point; (II) Cooling down to -100 °C at 5 °C /min. After thermal treatment, all samples were kept at ambient temperature.

RESULTS

SEM

Commercial AAO templates with a pore diameter of 100 nm and a length of 100 μm were used as closed end-pore templates. Figure 1 shows SEM images of broken AAO templates after the infiltration of the PBS homopolymer (a), the $BS_{78}CL_{22}$ random copolyester (b) and the PCL homopolymer (c). The SEM images clearly demonstrate that nanofiber structures were formed for all the samples. The diameter of the nanofibers is approximately 100 nm (see Figure SI-1 for a closer view), which agrees well with the diameter of the empty templates.

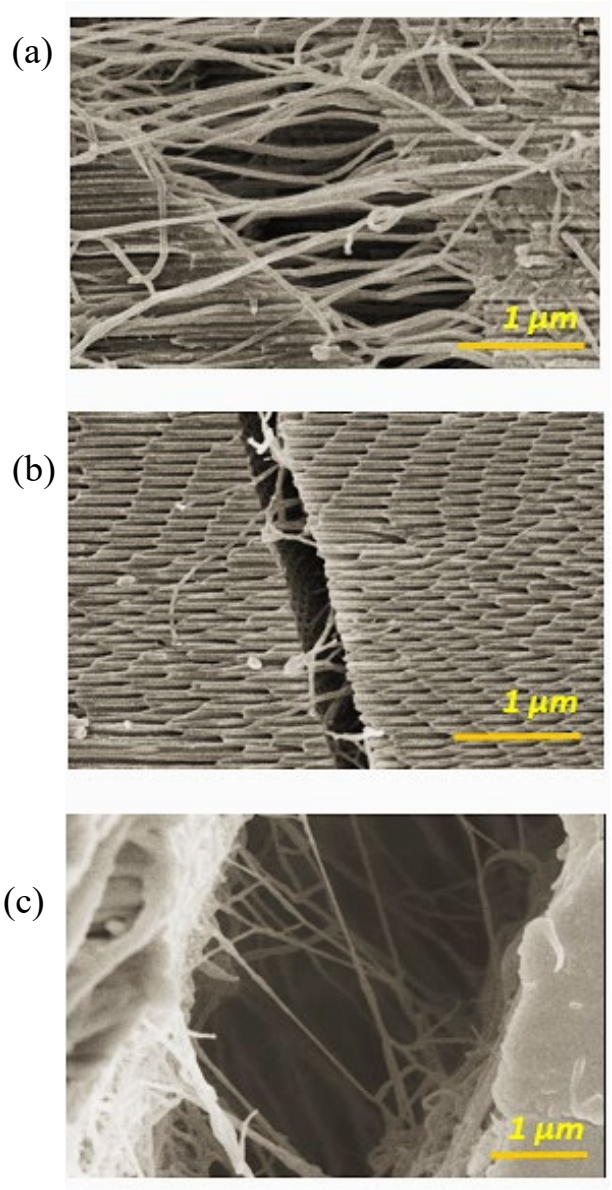

Figure 1. SEM micrographs of PBS homopolymer (a), $BS_{78}CL_{22}$ copolyester (b) and PCL homopolymer (c) nanofibers formed within the AAO templates after breaking the template using liquid nitrogen.

It should be noted that due to the lower rigidity of nanofibers in the compositions close to the pseudo-eutectic point, it was hard to physically extract nanofibers of AAO templates by breaking the template in liquid nitrogen. As an example, Figures 2a and 2b show top and cross-

section views of $BS_{45}CL_{55}$ that show that most pores are completely filled with polymer. In addition, there is an acceptable copolymer distribution along the pores (see Figure 2b). Figure SI-2 shows another example of an infiltrated copolymer near to the pseudo-eutectic composition, the $BS_{55}CL_{45}$ sample, which was also successfully infiltrated within the alumina nanotubes.

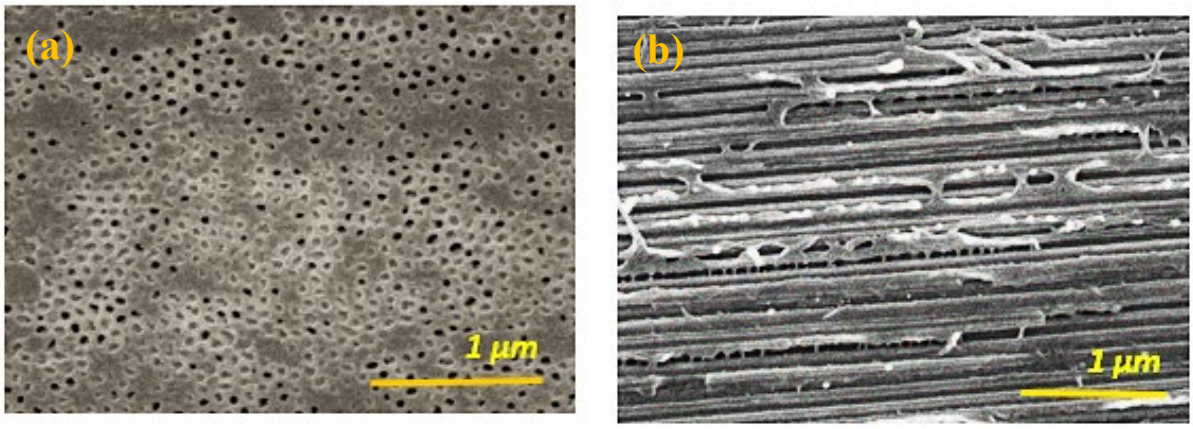

Figure 2. SEM micrographs of (a) the top-surface view of the infiltrated $BS_{45}CL_{55}$ copolymer inside the AAO template and (b) the cross-sectional view of the infiltrated $BS_{45}CL_{55}$ inside the AAO template.

Raman Spectroscopy

PBS and selected PBS-rich copolyesters in bulk and within AAO templates were examined by Raman spectroscopy to verify the infiltration penetration along the nanopores. Generally, the detected Raman spectra of bulk samples show less noise than infiltrated samples.

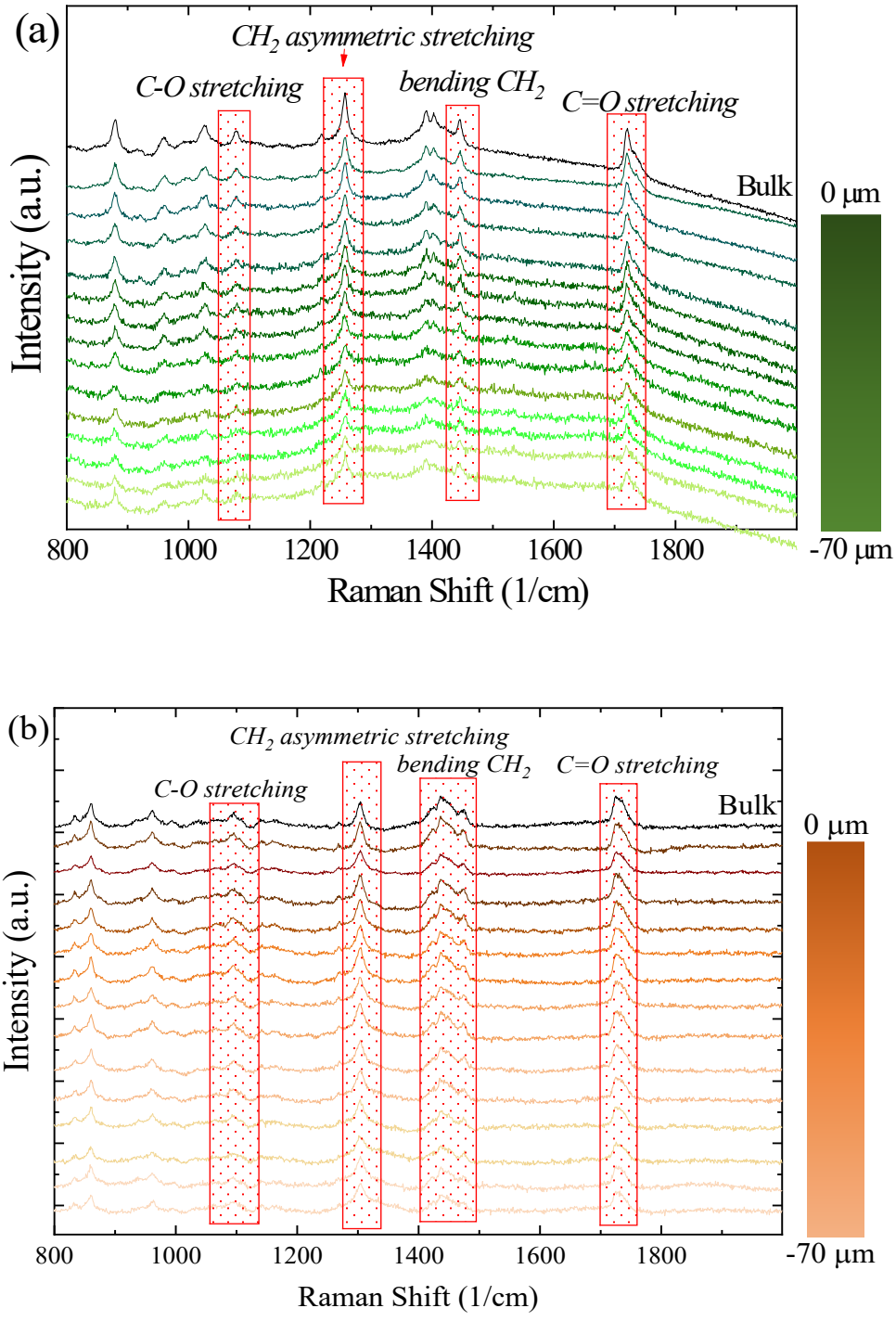

Figure 3. Normalized Raman spectra of infiltrated $BS_{78}CL_{22}$ (a) and $BS_{45}CL_{55}$ (b) samples within AAO templates along different depths.

Figures 3a and 3b show the normalized (by depth) Raman spectra of selected infiltrated samples: $BS_{78}CL_{22}$ and $BS_{45}CL_{55}$ compositions inside AAO templates, at different depths of up to 70 μm. The bands do not change with infiltration depth. This confirms that the PBS homopolymer and both copolymers infiltrated homogeneously within the nanocylinders.

Raman spectra of neat infiltrated $BS_{78}CL_{22}$ and $BS_{45}CL_{55}$ samples show the main specific bond vibrations of the PBS homopolymer, which, according to literature are [59]: around 1723 cm^{-1}, carbonyl bands stretching; at 1447 cm^{-1}, CH_2 in-plane bending; around 1256 cm^{-1}, CH_2 groups asymmetric stretching; and around 1080 cm^{-1}, stretching of the C-O bands.

The SEM images and the Raman results of the nanofibers clearly verify that the homopolymers and copolymers were completely infiltrated into the nanopores up to a depth of 70 μm. The templates we employed had 100 μm in depth, but complete filling was also qualitatively confirmed by alumina dissolution and later observing the nanofibers by SEM, although not shown here.

FT-IR Spectroscopy

In Figure 4, we show the FT-IR spectra of bulk and infiltrated homopolymers and two PBS-rich copolyesters ($BS_{78}CL_{22}$ and $BS_{45}CL_{55}$) in the 4000-500 cm^{-1} region. We can observe a decrease in band intensities of the infiltrated samples.

The infiltrated and bulk samples of the PBS-rich copolyesters (Figure 4a-c) exhibit characteristic bands of hydrocarbons groups at 2959 cm^{-1} and the carbonyl group vibrations at 1713 and 1738 cm^{-1} that are similar to those of neat PBS. Regarding the IR spectra of the PCL homopolymer (Figure 4d), we can identify the main strong bands such as the carbonyl stretching mode at 1722 cm^{-1}, the asymmetric CH_2 stretching at 2935 cm^{-1}, the symmetric CH_2 stretching

at 2856, the carbonyl stretching at 1718 cm^{-1} and the symmetric C-O-C stretching located at 1173 cm^{-1} [59].

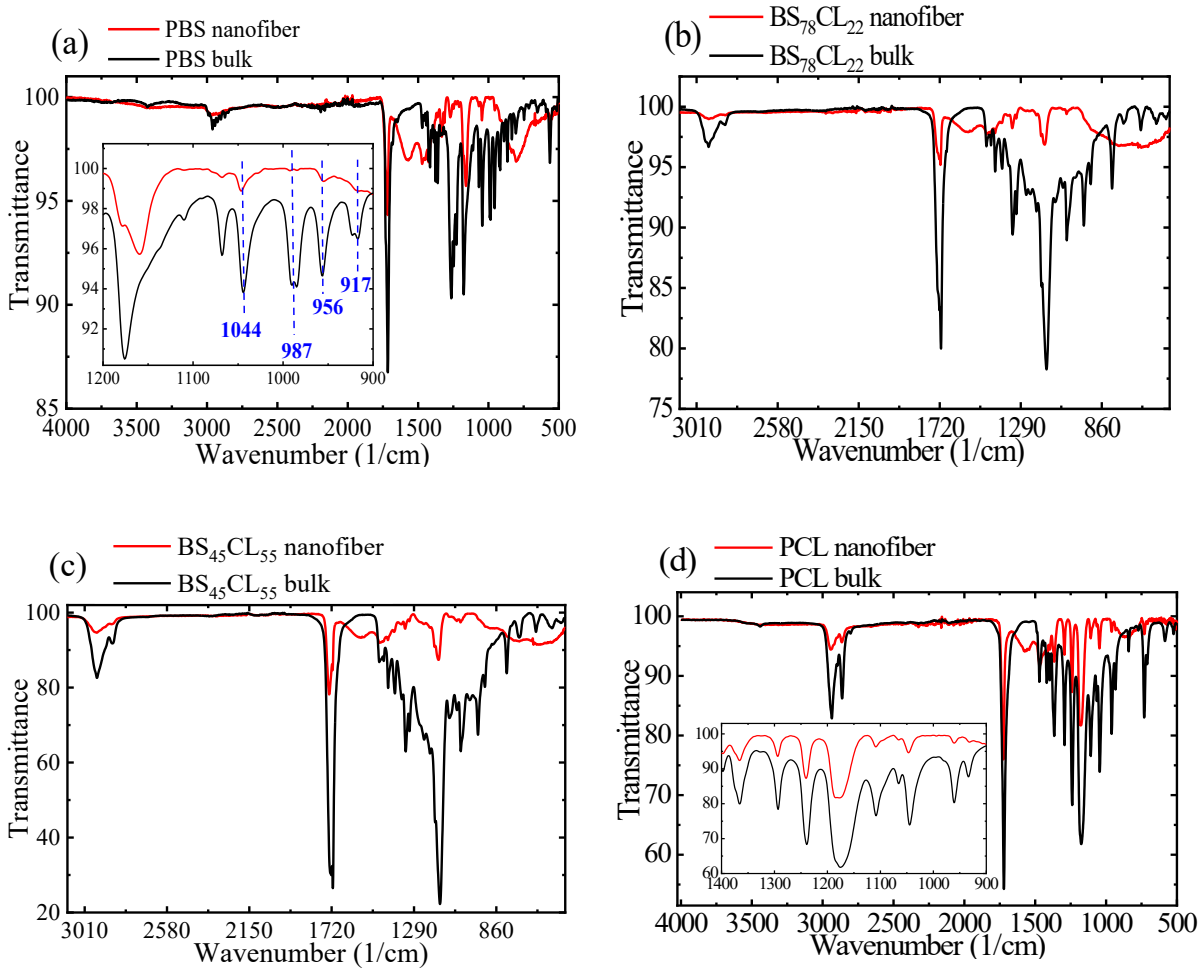

Figure 4. Infrared spectra of (a) PBS and (b) $BS_{78}CL_{22}$, (c) $BS_{45}CL_{55}$ and (d) PCL in bulk and infiltrated (nanofiber) within AAO 100 nm templates.

In addition, all PBS-rich copolyesters and PCL samples show a new band at around 1571 cm^{-1}, which arose from the stretching vibrations of carboxylic acid groups (COO^-) produced due to the existence of water molecules (released from the hydrolysis of ester groups) inside the nanopores[60,61].

One of the main changes observed in the IR spectra concerning bulk and infiltrated PBS-rich copolyesters is located around the 1200-800 cm^{-1} region. In the magnified area plotted as an inset in Figure 4a, four absorption bands associated to C−O single bonds can be detected for PBS homopolymer and PBS-rich copolymers. The band at 917 cm^{-1} can be assigned to C−OH bending vibrations and the bands at 987 and 956 cm^{-1} are due to the O−C stretching and vibration of ester groups. The signal at 1044 cm^{-1} corresponds to the stretching vibration of C−C−O groups. The intensity ratios of the C−C−O stretching and C−OH vibration peak to the intensity of the O−C stretching-peak in the nanofibers are higher than those in bulk samples. Moreover, the intensity ratio of the O−C−C stretching band to the intensity of the C−OH bending vibration is lower in the nanofibers than in the bulk sample. Similar results were obtained in our previous work for PBA and PBS polyesters[38]. These mentioned changes verify that confinement has an effect on the IR spectra. Actually, a smaller share of O−C bands was observed, which might possibly come from the interactions of PBS polymeric chains with the AAO walls.

In contrast, for the PCL homopolymer (see Figure 4d), the intensities of the peaks belonging to the C−O single bands located in the 1300-900 region, do not change in the confined sample, as compared to the bulk PCL.

The FTIR results demonstrate that for PBS-rich copolyesters nanofibers, there are new interactions between the polymer chains and the walls of the AAO templates, that are also present in the infiltrated PBS homopolymer. On the other hand, both PCL and PCL-rich copolymers do not show any detectable interaction with the AAO walls according to our FTIR results.

Figure 5 shows magnified IR spectra for the carbonyl stretching group bands of PBS-rich copolyesters at 1730 cm^{-1} that relate to the amorphous phase, and at 1715 cm^{-1} that correspond to the crystalline phase[62]. The ratio of the intensities of the amorphous phase band to the

crystalline phase band increases when the CL content in the copolymer increases. Therefore, the crystallinity degree decreases with comonomer content, as verified before by

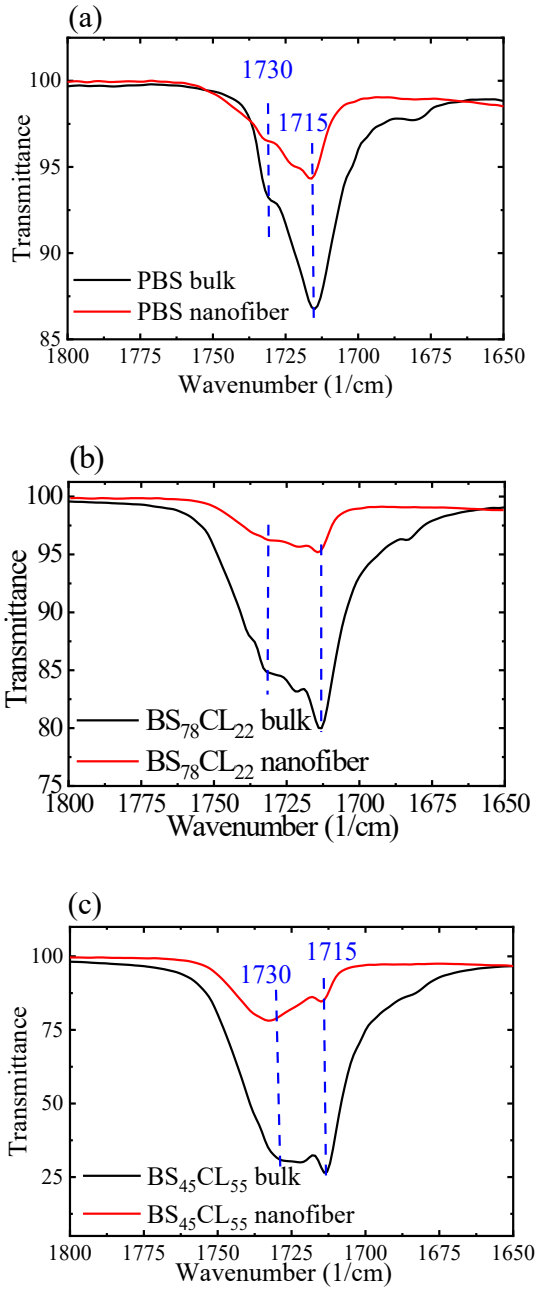

Figure 5. Infrared spectra of the bulk and infiltrated (nanofiber) PBS and PBS-rich copolyesters in the region of carbonyl group vibration for (a) PBS, (b) $BS_{78}CL_{22}$, and (c) $BS_{45}CL_{55}$.

DSC results in our previous works[57,58]. Moreover, the ratio of the amorphous phase band intensity to the crystalline phase band intensity increases under confinement, which also proves that the crystallinity degree decreases when the crystallization occurs inside the nanopores in all cases.

Non-Isothermal Crystallization

DSC scans of selected bulk samples and infiltrated ones inside 100 nm AAO templates are shown in Figure 6 (for PBS and PBS-rich copolyesters) and Figure 7 (for PCL and PCL-rich copolyesters). DSC scans for the rest of PBS-rich samples are shown in Figure SI-3. Data extracted from DSC curves are collected in Table SI-2.

Figures 6 and 7 show that during the cooling runs, bulk copolyesters exhibit crystallization peaks that depend on composition, as we have previously reported and analyzed in detail[57,58,63]. The novel results are those of infiltrated samples, in which a single crystallization peak can be generally observed at much lower temperatures than that detected in their corresponding bulk samples. These results indicate that all infiltrated polyesters and copolyesters are fully isolated within the nanopores without any interconnections because they do not display any crystallization exotherms at temperatures similar to the crystallization temperature of the corresponding bulk samples or any fractionated crystallization with multiple crystallization peaks [20-25,44,46,47].

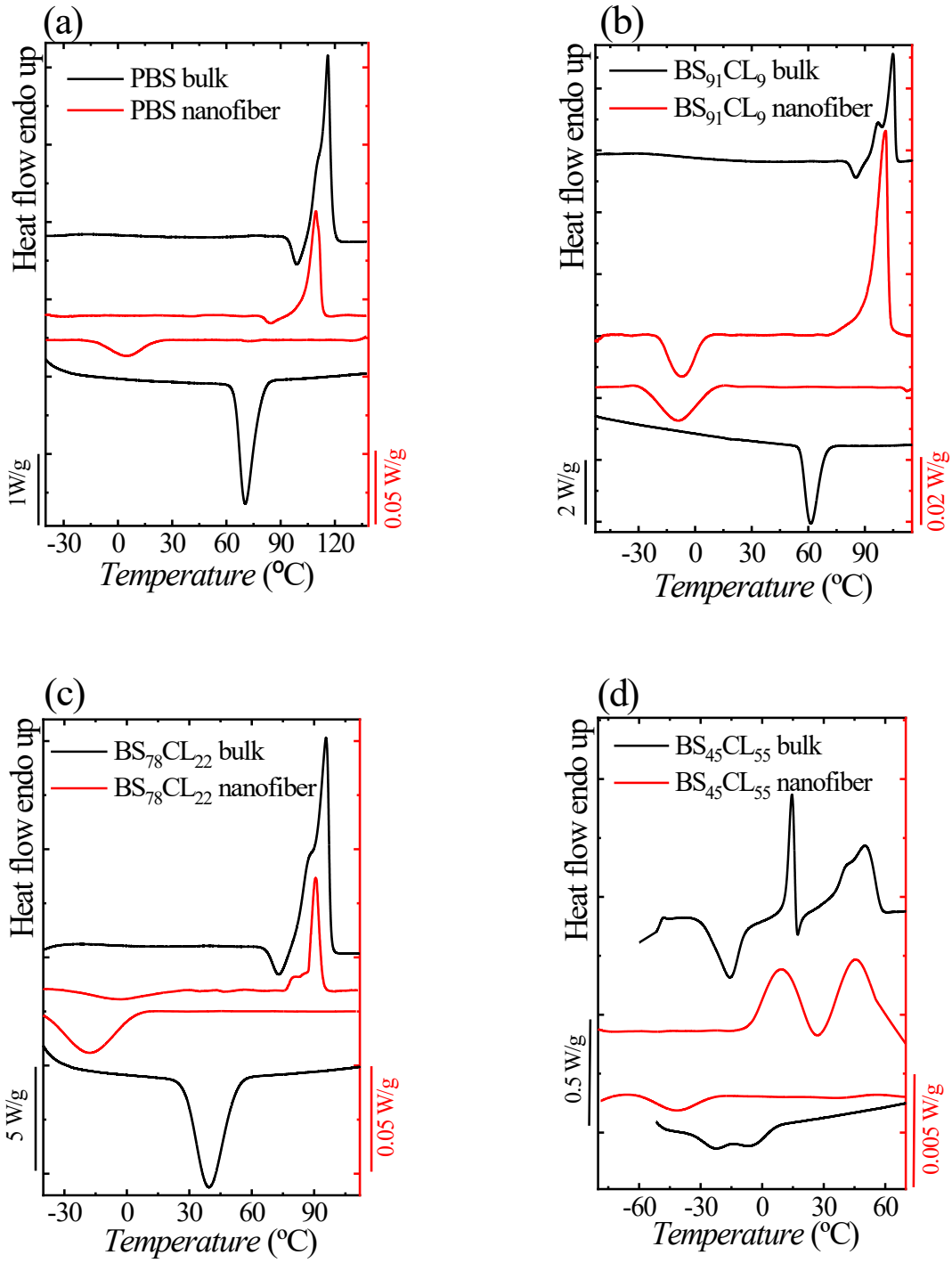

Figure 6. DSC cooling scans from the melt and subsequent heating scans for the indicated bulk and infiltrated (nanofibers) PBS homopolymer and PBS-rich copolyesters.

There are several orders of magnitude more nanopore cavities in the AAO templates (typically 10^{12} pores/cm^3) than heterogeneities in the bulk material (of the order of 10^6-10^8 heterogeneities/cm^3) before infiltration. Therefore, statistically the nanopores can be considered as heterogeneities free. Hence, the nucleation will proceed either by nucleation at the pore walls (surface nucleation) or by homogeneous nucleation inside the nanopore volume[17,20,27,64].

Some interesting peculiarities can be observed in Figure 6. Neat PBS in the bulk state (Figure 6a) shows a single crystallization exotherm upon cooling from the melt. Upon subsequent heating, the T_g can be observed at around -33 ºC, followed by a small but sharp cold crystallization exotherm just before the melting peak, a typical behavior of neat PBS.

The infiltrated PBS sample (Figure 6a) needs a much higher supercooling to crystallize (to be discussed below) and a melting behavior that is quite similar to that of the bulk sample preceded by a small cold crystallization exotherm. From the copolyester samples whose DSC scans are shown in Figure 6, two exhibit a rather similar behavior (see Figures 6b and 6c), as they display a single crystallization exotherm at very high supercooling (their peak crystallization temperatures are below -5 ºC) and then upon subsequent heating an extremely low temperature cold crystallization exotherm (in the same temperature range as the crystallization from the melt, i.e., below -5 ºC) very different to that of infiltrated neat PBS. In these samples, the contents of PBS in the copolymers are 91% (Figure 6b) and 78% (Figure 6c). The corresponding melting points of the infiltrated samples are always slightly lower than those of their bulk counterparts.

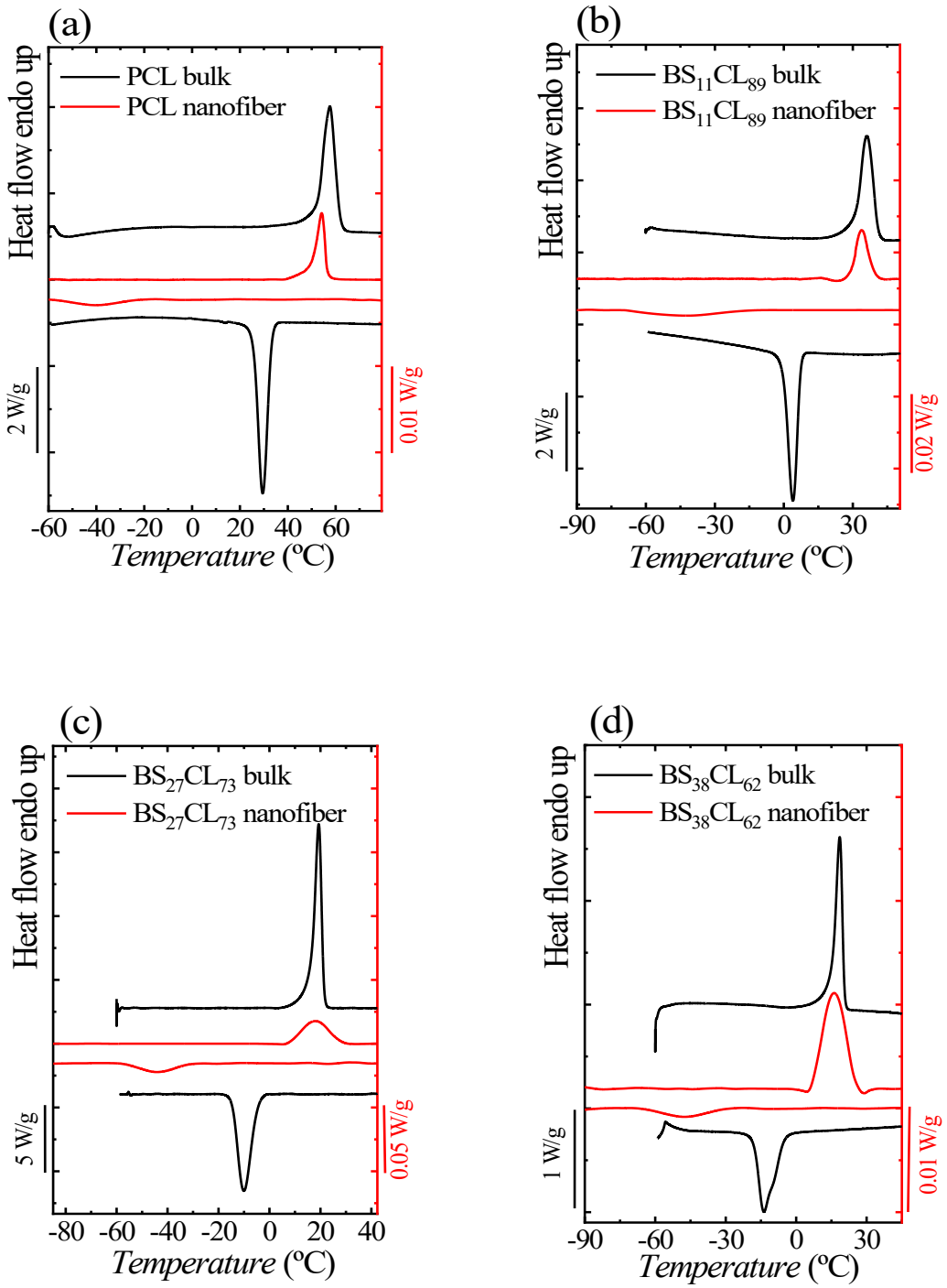

Figure 7. DSC cooling scans from the melt and subsequent heating scans for the indicated bulk and infiltrated (nanofibers) PCL homopolymer and PCL-rich copolyesters.

There is a special case shown in Figure 6 (see Figure 6d) for the copolyester whose composition coincides with the pseudo-eutectic point (i.e., $BS_{45}CL_{55}$), as this is the only sample where both PBS and PCL components can crystallize. This is shown in the plot of Figure 8, where T_c and T_m values are represented as a function of composition. The dashed vertical line in Figure 8a (or Figure 8b) shows the location of the pseudo-eutectic composition. To the left of this line, only PBS-rich phase crystals are formed, while to the right of this line PCL-rich phase crystals develop with crystal structures closely resembling PBS and PCL unit cells[57,58,63]. At the pseudo-eutectic composition, two crystalline phases can form and co-exist, i.e., PBS-rich and PCL-rich crystalline phases.

Going back to Figure 6d, the DSC scan (black solid line) for the bulk $BS_{45}CL_{55}$ sample upon cooling from the melt clearly shows two crystallization peaks (whose T_c values appear as two data points in Figure 8a), the first one for the PBS-rich phase at higher temperatures and the second one for the PCL-rich phase at lower temperatures.

The subsequent heating DSC scan (solid black line) in Figure 6d shows the following succession of thermal transitions upon increasing temperature: (a) an enthalpic heat capacity endothermic jump associated with the single T_g of this copolymer (at around -48 ºC); (b) a cold crystallization exotherm (at -16 ºC) of the PCL-rich phase; (c) a sharp melting endotherm corresponding mostly to the fusion of PCL-rich phase crystals with some overlap of the cold crystallization of the PBS-rich phase (whose sharp exothermic peak can be seen just after the melting peak of the PCL-rich phase crystals at around 13 ºC) and (d) the melting peak of the PBS-rich phase crystals at around 49 ºC.

In the same Figure 6d, but plotted in red lines, the DSC traces corresponding to the infiltrated $BS_{45}CL_{55}$ sample are shown. In the cooling DSC run, only one crystallization exotherm whose peak value is at approximately -41 ºC can be observed. In this single exotherm both phases crystallize coincidentally, as the subsequent heating run shows the two well defined melting endotherms corresponding to the fusion of PCL-rich phase and PBS-rich phase crystals.

Figure 7 shows results before and after infiltration for PCL homopolymer and PCL-rich copolyester samples. In this case, the behavior of all samples is very similar. Upon infiltration, all materials tend to crystallize at much lower temperatures (-40 ºC for the PCL homopolymer and lower temperatures for the copolymers) than in the corresponding bulk samples. In the case of their melting behavior, a slight decrease in melting points is observed for infiltrated samples.

As has been reported before, when the crystallization temperature is quite close to the glass transition temperature (T_g), the nucleation is almost certainly homogeneous [19,27,28,65]. In contrast, if a higher supercooling is needed for the crystallization of a confined polymer, as compared to the bulk polymer, but at substantially higher temperatures than the T_g value, surface-induced nucleation possibly controls the nucleation mechanism inside the nanopores. The T_c-T_g difference value in this work is therefore an indication of the relevant changes in nucleation mechanisms. The results presented in Figures 6 and 7 indicate that PBS-rich and PCL-rich copolyesters exhibit two different nucleation mechanisms, as explained in detail below.

The peak crystallization temperatures of infiltrated and bulk samples are plotted as a function of composition (expressed as mol% of CL units in the copolymer) in Figure 8a. The

large gap in peak crystallization temperature, T_c, between bulk and infiltrated samples demonstrates quantitatively the much larger supercooling (i.e., between 20 and 70 ºC depending on composition) needed to crystallize the infiltrated samples in AAO nanopores.

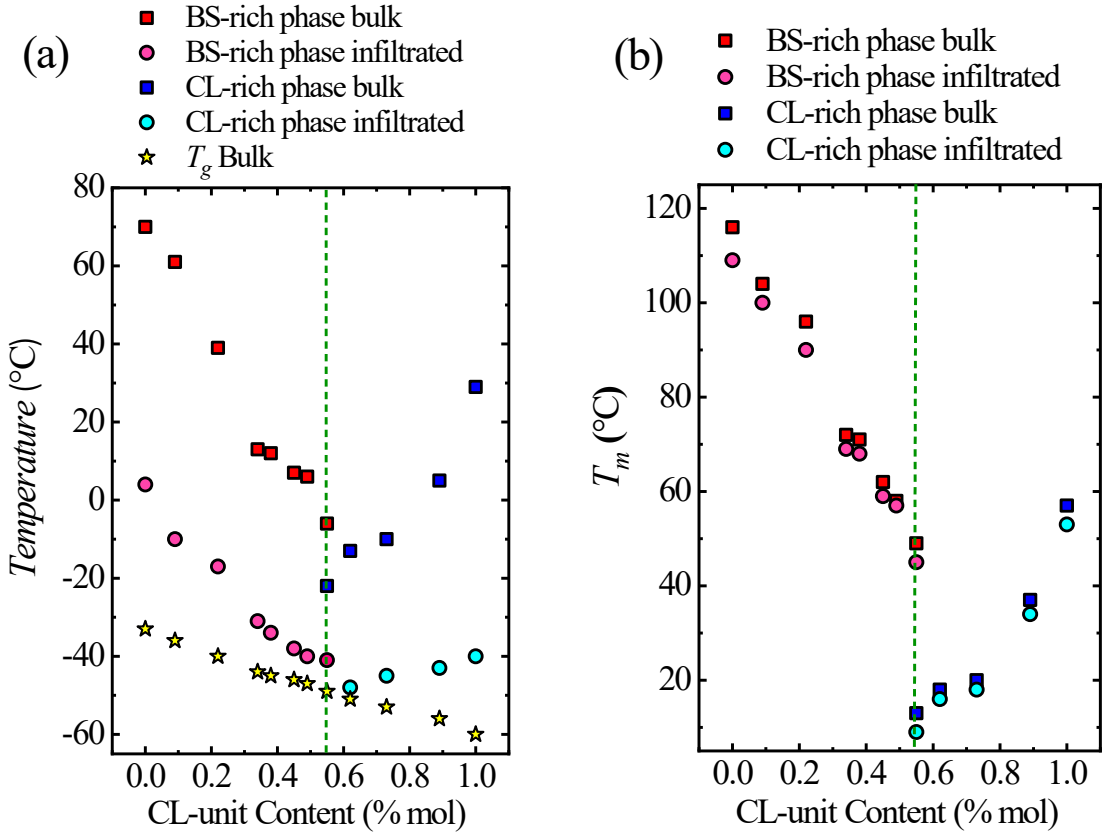

Figure 8. (a) Crystallization temperature, T_c, of bulk samples (squares), crystallization temperature, T_c, of infiltrated samples (circles) and glass transition temperature, T_g, of bulk samples (stars) as a function of CL content in the copolymers. (b) melting temperature peak, T_m, of bulk and infiltrated samples versus CL content in the copolymers. The segmented vertical lines indicate the position of the pseudo-eutectic point.

Figure 8 shows that both bulk and infiltrated samples exhibit a very clear pseudo-eutectic behavior corroborating the thermodynamic origin of the isodimorphism in these PBS-*ran*-PCL copolymers. In particular, when melting temperatures are examined, the behavior is

remarkably similar. Even though the crystallization is clearly much more difficult inside the nanopores and requires much higher supercoolings, the final outcome, at the unit cell level is the same. The trends in T_m versus composition are maintained, as the inclusion/exclusion ratio inside each of the PBS-rich or PCL-rich crystalline phases is still the same as in the bulk or inside the nanoporous confined volume. The isolated volume of the nanopores is small enough to impact the nucleation mechanism, but large enough so that no effect can be induced at the unit cell level (whose largest dimension is at least approximately two orders of magnitude smaller that the pore diameter).

If we first compare the change in T_c values upon infiltration for PBS and PCL homopolymers, it is clear that in the PCL case, the nucleation changes from heterogeneous (before infiltration) to homogeneous. Before infiltration, bulk PCL crystallizes in the range between 36 and 19 ºC, with a peak value of T_c=29 ºC. Infiltrated PCL in Figure 7a crystallizes is a much wider range, from -20 ºC down to -57 ºC, with a peak value at -40 ºC. Considering that the T_g value of bulk PCL is -60 ºC as determined by DSC, it is clear that PCL nanofibers inside the AAO nanopores crystallize in a range of temperatures that reach values that approach vitrification temperatures. This is a signature for homogeneous nucleation inside the nanopores volume. The occurrence of homogeneous nucleation of PCL under confinement has been reported previously[17,19,30,64,65]. According to the FTIR results presented above (see Figures 4 and 5), the PCL does not exhibit any interactions with the AAO pore walls, therefore, it cannot nucleate by a surface nucleation mechanism. Thus, the infiltrated PCL homopolymer has to create homogeneous nuclei by spontaneous aggregation of polymer chains inside the nanopores volume, a process that requires surpassing a high energy barrier, hence it needs the maximum possible supercooling before vitrification[44,46].

On the other hand, the PBS homopolymer (Figure 6a) displays a different behavior. PBS has a T_g value of approximately -33 ºC. The bulk material crystallizes upon cooling from the melt in a range between 87 ºC and 60 ºC, with an exothermic peak at 70 ºC. When PBS is confined within the AAO nanopores, its crystallization range starts at 21 ºC down to -16 ºC, with a peak value of 4 ºC. Its peak crystallization value is 37 ºC higher than the T_g, while the lowest detected crystallization upon cooling is at 17 ºC higher than T_g. Therefore, it is more plausible that the nucleation in the PBS case changes from heterogeneous (before infiltration) to a surface-induced nucleation. The FTIR results presented above (see Figures 4 and 5) indicate that PBS presents interactions with the AAO walls, therefore supporting a surface nucleation mechanism for the infiltrated PBS homopolymer.

Remarkably, the PBS-rich and PCL-rich copolyesters show different trends with increasing amounts of comonomer in Figure 8a. The trend exhibited by the values of T_c (crystallization peak values) as a function of composition for the infiltrated samples should be compared with the plotted T_g values measured by DSC in bulk samples.

To the left of the pseudo-eutectic point in Figure 8a, where the PBS-rich copolyesters are located, the nucleation mechanism changes from surface nucleation, for PBS homopolymer, to homogeneous nucleation, for the $BS_{45}CL_{55}$ copolymer. The difference between the crystallization and the glass transition temperatures of BS-rich compositions shows that by adding CL-comonomer, the nucleation mechanism progressively turns to homogenous nucleation. This is probably caused by a dilution effect on the PBS chains-AAO walls interactions, as PCL content in the copolymers increases. For instance, the T_c value of the infiltrated PBS homopolymer is 37 °C above its T_g temperature, but the T_c value of the infiltrated composition with 34 % of CL is about 14 °C above its T_g value, and for the

composition at the pseudo-eutectic point, which has 55% CL content, it is only 7 °C above their corresponding T_g temperature. In fact, Figure 6d shows the overlap between the T_g of bulk $BS_{45}CL_{55}$ and the end of the crystallization exotherm for the infiltrated $BS_{45}CL_{55}$ sample.

On the other hand, all the compositions that are rich in PCL exhibit a homogenous nucleation mechanism. Even though the peak crystallization temperature T_c for PCL decreases with PBS content in the copolymer (Figure 8a), the end of the crystallization range in all PCL rich samples is located around -60 ºC in Figure 7. We include a low temperature range close-up of Figures 6 and 7 in the Supplementary Information (Figure SI-4), where the differences between crystallization temperature ranges and T_g values (and T_g ranges) can be clearly appreciated.

Subsequent heating scans (see Figure 8b) demonstrate that the melting points of confined copolyesters are somewhat lower at all compositions as compared to the bulk values (around 3-7 °C, the large range of temperatures in the y-axis of the figures makes difficult to appreciate these small differences, but the values are listed in Table SI-2 of the SI). It is expected that the confined materials that crystallize at much lower temperatures than the bulk samples, form thinner lamellae that melt correspondingly at lower temperatures.

Crystalline Structure of PBS-*ran*-PCL within Nanopores

2D grazing incidence WAXS experiments were performed at ambient temperature to study the orientation and texture of the copolyesters crystals inside the AAO nanopores. Samples for GIWAXS measurements were heated to 30 ºC above their corresponding melting temperatures and then cooled down at 5 °C/min to allow them to crystallize.

Figures 9a-h show GIWAXS patterns for the bulk and infiltrated PBS-rich samples. There are three separate reflections for the PBS sample at q =13.9, 15.3 and 15.9 nm^{-1}. These reflections have d-spacing values of 4.52, 4.11 and 3.95 Å, which can be assigned to the following crystal planes: (020)/($\bar{1}$11), (021), and (110), respectively. For the infiltrated PBS-rich phase, only two main reflections were detected at q = 13.8 and 15.9 nm^{-1} that can be indexed as the (020)/($\bar{1}$11) and (110)/(021) reflections. Figures 10a-d show the corresponding 1-D scattering patterns determined from the data in Figure 9. These results show that both bulk and infiltrated homopolymers and BS-rich copolymers crystallized in the same α form. There is no polymorphic transformation for the PBS crystalline phase upon infiltration. Similar results were observed in our previous work for PBS homopolymer infiltrated in a 70 nm AAO template[38].

Figures 11a-d show the GIWAXS patterns of bulk and infiltrated PCL-rich copolyesters at room temperature. For the PCL bulk homopolymer, major reflections were observed at q = 15.1, 15.6, and 16.7 nm^{-1}, and they correspond to d-spacing values of 4.16, 4.02, and 3.77 Å, respectively. The corresponding 1D GIWAXS patterns are plotted in Figure 12. The reflections of the (200), (111), and (110) planes can be observed, which can be assigned to the PCL orthorhombic unit cell, as reported by Chatani *et al*.[66]. We observed that the crystal form of PCL does not change within 100 nm nanopores as previously reported by Shi *et al*.[64] for confined PCL inside 100 nm AAO pores. Among the PCL-rich compositions, we could measure GIWAXS for the $BS_{11}CL_{89}$ sample, because this composition is the only one that is not molten at room temperature and it shows reflections that are very close to those of the PCL homopolymer (see Figures 11c-d and 12b).

As in the AAO template the amount of polymer is smaller and the crystallinity degree is poorer in all the cases, these samples show weaker intensities within the AAO templates than in bulk.

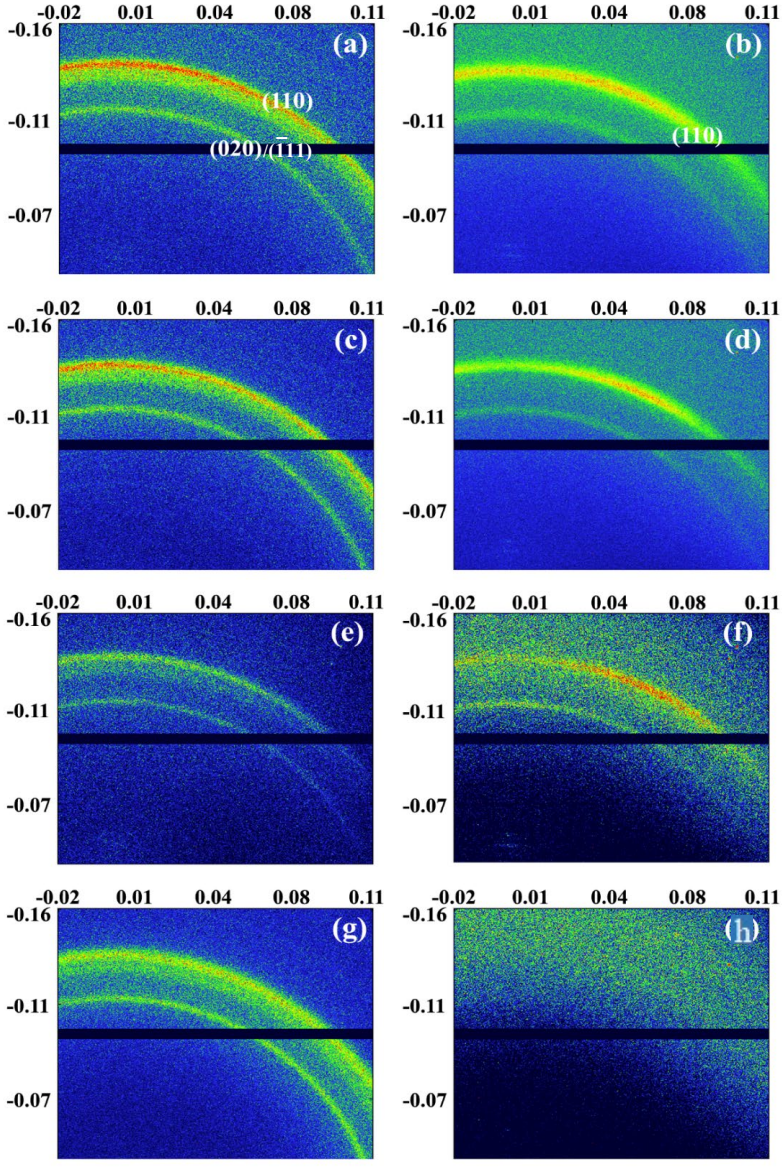

Figure 9. 2D grazing incidence WAXS patterns for samples of (a) bulk PBS, (b) infiltrated PBS, (c) bulk $BS_{91}CL_9$, (d) infiltrated $BS_{91}CL_9$, (e) bulk $BS_{78}CL_{22}$, (f) infiltrated $BS_{78}CL_{22}$, (g) bulk $BS_{66}CL_{34}$ and (h) infiltrated $BS_{66}CL_{34}$.

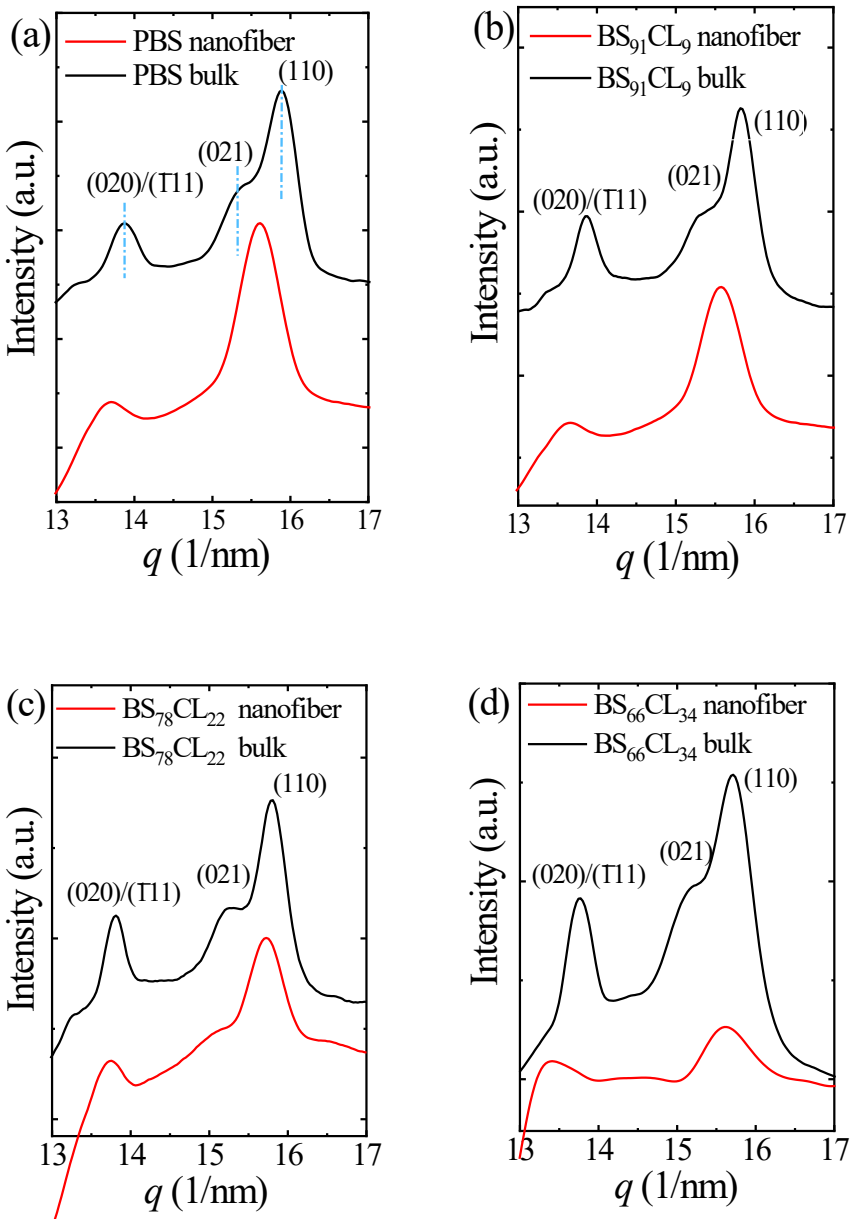

Figure 10. Corresponding 1D GIWAXS patterns of bulk and infiltrated (nanofibers) samples of (a) PBS, (b) $BS_{91}CL_9$, (c) $BS_{78}CL_{22}$ and (d) $BS_{66}CL_{34}$.

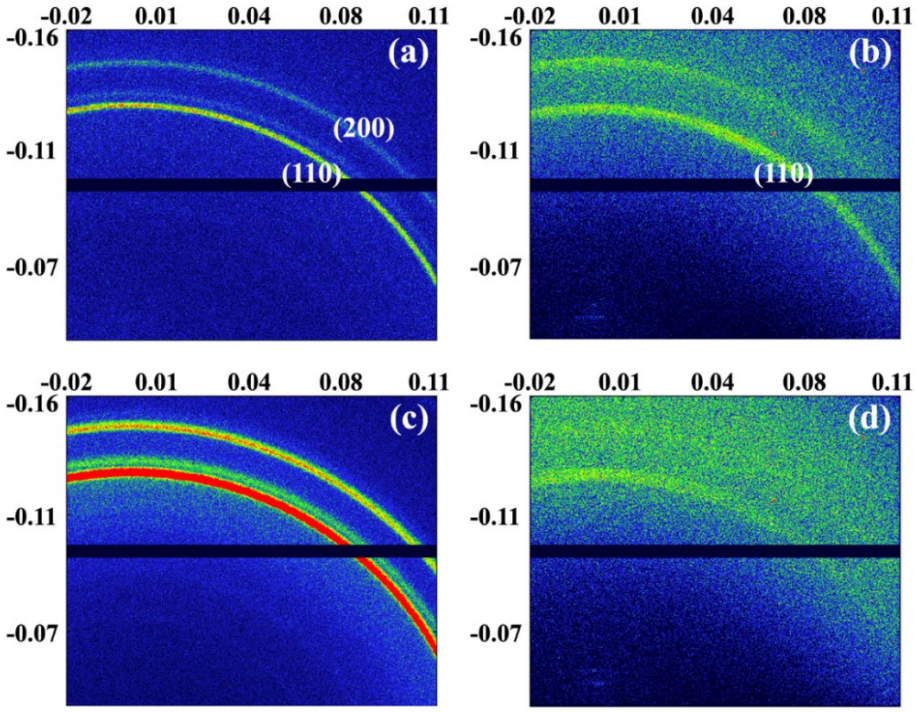

Figure 11. 2D WAXS patterns for samples of (a) bulk PCL, (b) infiltrated PCL, (c) bulk $BS_{11}CL_{89}$, and (d) infiltrated $BS_{11}CL_{89}$.

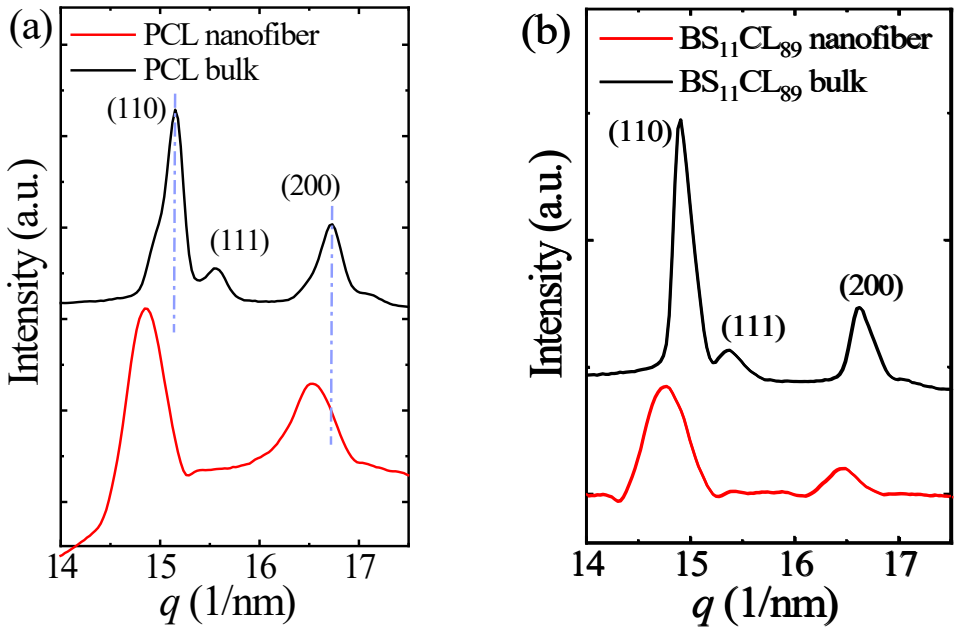

Figure 12. Corresponding 1D GIWAXS patterns of bulk and infiltrated (nanofibers) samples of (a) PCL and (b) $BS_{11}CL_{89}$.

Polymers within AAO often exhibit anisotropic crystal growth during crystallization. The orientation depends on the kinetics of nucleation and growth[29,32]. The degree of anisotropy of PBS-rich polymer is quite low, similar to a previous study[38]. As shown in Figure 9, a clear feature of the 2D patterns of PBS-rich copolymer is the off-meridian maxima of the (110) peak (azimuth ~25º). The azimuthal intensity profiles of PBS-rich polymers were plotted in Figure SI-5. According to the unit cell parameters of PBS (a = 0.523 nm, b = 0.912 nm, c = 1.090 nm, and β = 123.98° [67]), the angle of ~ 25º agrees with the angle between the (020) plane and (021) plane (26.8º). Therefore, the orientation mode of PBS-rich copolymers can be assigned as the (020) plane perpendicular to the pore axis.

As for PCL-rich copolymers, since the scattering signal is weak, the assignment of the orientation mode is difficult. Nevertheless, the orientation of PCL has been studied extensively in a previous study[64].

CONCLUSIONS

This study demonstrated that polyester nanofibers were successfully made from PBS and PCL homopolymers and PBS-*ran*-PCL random copolymers over the entire range of compositions by infiltrating into AAO templates. All compositions, even at the pseudo-eutectic point, were able to crystallize within the nanopores. However, the crystallization temperature decreased significantly under confinement and both the infiltrated copolyesters and the bulk copolyesters showed an identical pseudo-eutectic behavior. The nucleation mechanism was composition-dependent, as judged by the difference between the crystallization temperature and the glass transition temperature.

Interactions between PBS chains and AAO walls were identified by FTIR results, supporting the surface nucleation mechanism that was exhibited by neat PBS. In the case of PBS-rich samples, a probable shift from surface nucleation, for the PBS homopolymer, to homogeneous nucleation, for compositions near to the pseudo-eutectic point, was assigned. This shift is probably due to the progressive dilution of the PBS/AAO walls interactions in the copolymers, as the PCL content in the copolymers increased. In contrast, for the infiltrated PCL and PCL-rich copolyesters, a homogenous nucleation mechanism is more probable in all cases. FTIR showed that the PCL homopolymer does not show any affinity with the AAO walls, a result that explains the predominance of homogeneous nucleation inside the volume of the nanopores for PCL and PCL rich copolyesters, where only the PCL phase can crystallize.

The crystalline modifications of the copolyesters kept unchanged after infiltration. The degree of anisotropy of all the samples was low, suggesting high nucleation density inside the nanodomains crystallized at high supercoolings. Low degrees of orientation were seen for all

the samples and the orientation mode of the copolyesters is very similar to that of the infiltrated homopolymers of dominant comonomers.

ACKNOWLEDGMENTS

We acknowledge the support of the National Key R&D Program of China (2017YFE0117800), the National Natural Science Foundation of China (21873109, 51820105005). We would also like to thank the financial support provided by the BIODEST project; this project has received funding from the European Union's Horizon 2020 research and innovation programme under the Marie Skłodowska-Curie grant agreement No 778092. The UPV/EHU and ICTP-CSIC Institutions acknowledge financial support from the Spanish Ministry of Science, Innovation, and Universities (MAT2017-83014-C2-2-P and MAT2017-83014-C2-1-P). M.S. thankfully acknowledges her Ph.D. fellowship by POLYMAT Basque Center for Macromolecular Design and Engineering. Authors would like to thank Dr. Antxon Martinez de Ilarduya and Prof. Sebastian Muñoz for their help in the synthesis of copolyesters at UPC, Spain. J.M. gratefully acknowledges support from the Provincial Council of Gipuzkoa under the program Fellow Gipuzkoa and “Fomento San Sebastián” in the framework program “Retorno del Talento Local” Donostia up! 2016.

Supporting Information

SEM micrographs (Figures SI-1 and SI-2), DSC curves (Figures SI-3 and SI-4), Azimuthal intensity profiles (Figure SI-5); GPC and DSC data (Tables SI-1 and Table SI-2).

REFERENCES

(1) Andrews, D.; Nann, T.; Lipson, R. H., *Comprehensive Nanoscience and Nanotechnology*. 2 ed.; Academic Press: Cambridge, 2019.

(2) Zhang, L.; Webster, T. J. Nanotechnology and nanomaterials: promises for improved tissue regeneration. *Nano today* **2009**, 4 (1), 66-80, DOI: 10.1016/j.nantod.2008.10.014.

(3) Martin, J.; Maiz, J.; Sacristan, J.; Mijangos, C. Tailored polymer-based nanorods and nanotubes by" template synthesis": From preparation to applications. *Polymer* **2012**, 53 (6), 1149-1166, DOI: 10.1016/j.polymer.2012.01.028.

(4) Hernández, J. J.; Puente-Orench, I.; Ezquerra, T. A.; Gutiérrez-Fernández, E.; García-Gutiérrez, M.-C. Confinement effects in one-dimensional nanoarrays of polymer semiconductors and their photovoltaic blends. *Polymer* **2019**, 163, 13-19, DOI: 10.1016/j.polymer.2018.12.036.

(5) Adrjanowicz, K.; Winkler, R.; Dzienia, A.; Paluch, M.; Napolitano, S. Connecting 1D and 2D Confined Polymer Dynamics to Its Bulk Behavior via Density Scaling. *ACS. macro. lett*. **2019**, 8 (3), 304-309, DOI: 10.1021/acsmacrolett.8b01006.

(6) Sayin, S.; Ozdemir, E.; Acar, E.; Ince, G. O. Multifunctional one-dimensional polymeric nanostructures for drug delivery and biosensor applications. *Nanotechnology* **2019**, 30 (41), 412001, DOI: 10.1088/1361-6528/ab2e2c.

(7) Xu, Q.; Meng, G.; Han, F. Porous AAO template-assisted rational synthesis of large-scale 1D hybrid and hierarchically branched nanoarchitectures. *Prog. Mater. Sci.* **2018**, 95, 243-285, DOI: 10.1016/j.pmatsci.2018.02.004.

(8) Martin, J.; Krutyeva, M.; Monkenbusch, M.; Arbe, A.; Allgaier, J.; Radulescu, A.; Falus, P.; Maiz, J.; Mijangos, C.; Colmenero, J. Direct observation of confined single chain dynamics by neutron scattering. *Phys. rev. lett.* **2010**, 104 (19), 197801, DOI: 10.1103/PhysRevLett.104.197801.

(9) Zhang, X.; Liu, H.; Jiang, L. Wettability and applications of nanochannels. *Adv. Mater.* **2019**, 31 (5), 1804508, DOI: 10.1002/adma.201804508.

(10) Rath, A.; Theato, P. Advanced AAO Templating of Nanostructured Stimuli-Responsive Polymers: Hype or Hope? *Adv. Funct. Mater.* **2020**, 30, 1902959, DOI: 10.1002/adfm.201902959.

(11) Sanz, B.; Ballard, N.; Marcos-Fernandez, A.; Asua, J. M.; Mijangos, C. Confinement effects in the step-growth polymerization within AAO templates and modeling. *Polymer* **2018**, 140, 131-139, DOI: 10.1016/j.polymer.2018.02.041.

(12) Müller, A. J.; Arnal, M. L.; Trujillo, M.; Lorenzo, A. T. Super-nucleation in nanocomposites and confinement effects on the crystallizable components within block copolymers, miktoarm star copolymers and nanocomposites. *Eur. Polym. J.* **2011**, 47 (4), 614-629, DOI: 10.1016/j.eurpolymj.2010.09.027.

(13) Frensch, H.; Harnischfeger, P.; Jungnickel, B., *Fractionated crystallization in incompatible polymer blends*. ACS Symposium Series, American Chemical Society: Washington, 1989; Vol. 395.

(14) Hamley, I., Crystallization in block copolymers. In *Interfaces Crystallization Viscoelasticity*, Springer: Berlin, Germany, 1999; Vol. 148, pp 113-137.

(15) Hamley, I. W., *Developments in block copolymer science and technology*. John Wiley & Sons: New York, 2004.

(16) Loo, Y. L.; Register, R. A., *Crystallization within block copolymer mesophases*. Wiley: New York, 2004.

(17) Müller, A. J.; Arnal, M. L.; Balsamo, V., Crystallization in block copolymers with more than one crystallizable block. In *Progress in understanding of polymer crystallization*, Reiter, G., Strobl, G., Eds. Springer: Berlin, Germany, 2007; Vol. 714, pp 229-259.

(18) Müller, A. J.; Arnal, M. L.; Lorenzo, A. T., *Crystallization in nano-confined polymeric systems*. Wiley: New York, 2013; Vol. 1.

(19) Michell, R. M.; Blaszczyk-Lezak, I.; Mijangos, C.; Müller, A. J. Confinement effects on polymer crystallization: From droplets to alumina nanopores. *Polymer* **2013**, 54 (16), 4059-4077, DOI: 10.1016/j.polymer.2013.05.029.

(20) Michell, R. M.; Lorenzo, A. T.; Müller, A. J.; Lin, M.-C.; Chen, H.-L.; Blaszczyk-Lezak, I.; Martin, J.; Mijangos, C. The crystallization of confined polymers and block copolymers infiltrated within alumina nanotube templates. *Macromolecules* **2012**, 45 (3), 1517-1528, DOI: 10.1021/ma202327f.

(21) Casas, M. T.; Michell, R. M.; Blaszczyk-Lezak, I.; Puiggali, J.; Mijangos, C.; Lorenzo, A. T.; Müller, A. J. Self-assembly of semicrystalline PE-b-PS diblock copolymers within AAO nanoporous templates. *Polymer* **2015**, 70, 282-289, DOI: 10.1016/j.polymer.2015.06.025.

(22) Chen, D.; Chen, J. T.; Glogowski, E.; Emrick, T.; Russell, T. P. Thin film instabilities in blends under cylindrical confinement. *Macromol. Rapid Commun.* **2009**, 30 (4-5), 377-383, DOI: 10.1002/marc.200800730.

(23) Xu, J.; Wang, K.; Liang, R.; Yang, Y.; Zhou, H.; Xie, X.; Zhu, J. Structural transformation of diblock copolymer/homopolymer assemblies by tuning cylindrical confinement and interfacial interactions. *Langmuir* **2015**, 31 (45), 12354-12361, DOI:10.1021/acs.langmuir.5b03146.

(24) Duran, H.; Steinhart, M.; Butt, H.-J.; Floudas, G. From heterogeneous to homogeneous nucleation of isotactic poly (propylene) confined to nanoporous alumina. *Nano Lett.* **2011**, 11 (4), 1671-1675, DOI: 10.1021/nl200153c.

(25) Liu, C.-L.; Chen, H.-L. Crystal orientation of PEO confined within the nanorod templated by AAO nanochannels. *Soft matter* **2018**, 14 (26), 5461-5468, DOI: 10.1039/C8SM00795K.

(26) Wu, H.; Higaki, Y.; Takahara, A. Molecular self-assembly of one-dimensional polymer nanostructures in nanopores of anodic alumina oxide templates. *Prog. Polym. Sci.* **2018**, 77, 95-117, DOI: 10.1016/j.progpolymsci.2017.10.004.

(27) Michell, R. M.; Blaszczyk-Lezak, I.; Mijangos, C.; Müller, A. J. Confined crystallization of polymers within anodic aluminum oxide templates. *J. Polym. Sci. Pol. Phys.* **2014**, 52 (18), 1179-1194, DOI: 10.1002/polb.23553.

(28) Michell, R. M.; Müller, A. J. Confined crystallization of polymeric materials. *Prog. Polym. Sci.* **2016**, 54, 183-213, DOI: 10.1016/j.progpolymsci.2015.10.007.

(29) Su, C.; Shi, G.; Wang, D.; Liu, G. A Model for the Crystal Orientation of Polymers Confined in 1D Nanocylinders. *Acta. Polym. Sin.* **2019**, 50 (3), 281-290, DOI: 10.11777/j.issn1000-3304.2019.18218.

(30) Suzuki, Y.; Duran, H.; Akram, W.; Steinhart, M.; Floudas, G.; Butt, H.-J. Multiple nucleation events and local dynamics of poly (ε-caprolactone)(PCL) confined to nanoporous alumina. *Soft Matter* **2013**, 9 (38), 9189-9198, DOI: 10.1039/C3SM50907A.

(31) Shin, K.; Woo, E.; Jeong, Y. G.; Kim, C.; Huh, J.; Kim, K.-W. Crystalline structures, melting, and crystallization of linear polyethylene in cylindrical nanopores. *Macromolecules* **2007**, 40 (18), 6617-6623, DOI: 10.1021/ma070994e.

(32) Steinhart, M.; Göring, P.; Dernaika, H.; Prabhukaran, M.; Gösele, U.; Hempel, E.; Thurn-Albrecht, T. Coherent kinetic control over crystal orientation in macroscopic ensembles of polymer nanorods and nanotubes. *Phys. Rev. Lett.* **2006**, 97 (2), 027801, DOI: 10.1103/PhysRevLett.97.027801.

(33) Wu, H.; Higaki, Y.; Nojima, S.; Takahara, A. Orientation and crystallization of regioregular poly (3-dodecylthiophene) in alumina nanopores. *Soft matter* **2017**, 13 (26), 4661-4666, DOI: 10.1039/C7SM00859G.

(34) Su, C.; Shi, G.; Li, X.; Zhang, X.; Müller, A. J.; Wang, D.; Liu, G. Uniaxial and Mixed Orientations of Poly (ethylene oxide) in Nanoporous Alumina Studied by X-ray Pole Figure Analysis. *Macromolecules* **2018**, 51 (23), 9484-9493, DOI:10.1021/acs.macromol.8b01801.

(35) Su, C.; Chen, Y.; Shi, G.; Li, T.; Liu, G.; Müller, A. J.; Wang, D. Crystallization Kinetics of Poly (ethylene oxide) under Confinement in Nanoporous Alumina Studied by in Situ X-ray Scattering and Simulation. *Langmuir* **2019**, 35 (36), 11799-11808, DOI: 10.1021/acs.langmuir.9b01968.

(36) Guan, Y.; Liu, G.; Ding, G.; Yang, T.; Müller, A. J.; Wang, D. Enhanced crystallization from the glassy state of poly (L-lactic acid) confined in anodic alumina oxide nanopores. *Macromolecules* **2015**, 48 (8), 2526-2533, DOI:10.1021/acs.macromol.5b00108.

(37) Li, L.; Liu, J.; Qin, L.; Zhang, C.; Sha, Y.; Jiang, J.; Wang, X.; Chen, W.; Xue, G.; Zhou, D. Crystallization kinetics of syndiotactic polypropylene confined in nanoporous alumina. *Polymer* **2017**, 110, 273-283, DOI: 10.1016/j.polymer.2016.12.081.

(38) Safari, M.; Maiz, J.; Shi, G.; Juanes, D.; Liu, G.; Wang, D.; Mijangos, C.; Alegría, A. n.; Müller, A. J. How Confinement Affects the Nucleation, Crystallization, and Dielectric Relaxation of Poly (butylene succinate) and Poly (butylene adipate) Infiltrated within Nanoporous Alumina Templates. *Langmuir* **2019**, 35 (47), 15168-15179, DOI: 10.1021/acs.langmuir.9b02215.

(39) Wu, H.; Wang, W.; Yang, H.; Su, Z. Crystallization and orientation of syndiotactic polystyrene in nanorods. *Macromolecules* **2007**, 40 (12), 4244-4249, DOI: 10.1021/ma070564o.

(40) Yu, S.; Lai, Z.; Jinnai, H.; Zeng, X.; Ageishi, M.; Lotz, B.; Cheng, S. Z.; Zheng, N.; Zhang, S.; Feng, X. Adding Symmetry: Cylindrically Confined Crystallization of Nylon-6. *Macromolecules* **2019**, 52 (9), 3298-3305, DOI: 10.1021/acs.macromol.8b02672.

(41) Dai, X.; Li, H.; Ren, Z.; Russell, T. P.; Yan, S.; Sun, X. Confinement Effects on the Crystallization of Poly (3-hydroxybutyrate). *Macromolecules* **2018**, 51 (15), 5732-5741, DOI: 10.1021/acs.macromol.8b01083.

(42) Li, L.; Zhou, D.; Huang, D.; Xue, G. Double glass transition temperatures of poly (methyl methacrylate) confined in alumina nanotube templates. *Macromolecules* **2014**, 47 (1), 297-303, DOI: 10.1021/ma4020017.

(43) Li, L.; Raghupathi, K.; Song, C.; Prasad, P.; Thayumanavan, S. Self-assembly of random copolymers. *ChemComm* **2014**, 50 (88), 13417-13432, DOI: 10.1039/C4CC03688C.

(44) Papageorgiou, G. Z.; Bikiaris, D. N. Synthesis and Properties of Novel Biodegradable/Biocompatible Poly [propylene-co-(ethylene succinate)] Random Copolyesters. *Macromol. Chem. Phys.* **2009**, 210 (17), 1408-1421, DOI: 10.1002/macp.200900132.

(45) Pérez-Camargo, R. A.; Fernández-d'Arlas, B.; Cavallo, D.; Debuissy, T.; Pollet, E.; Avérous, L.; Müller, A. J. Tailoring the structure, morphology, and crystallization of isodimorphic poly (butylene succinate-ran-butylene adipate) random copolymers by changing composition and thermal history. *Macromolecules* **2017**, 50 (2), 597-608, DOI: 10.1021/acs.macromol.6b02457.

(46) Yu, Y.; Sang, L.; Wei, Z.; Leng, X.; Li, Y. Unique isodimorphism and isomorphism behaviors of even-odd poly (hexamethylene dicarboxylate) aliphatic copolyesters. *Polymer* **2017**, 115, 106-117, DOI: 10.1016/j.polymer.2017.03.034.

(47) Arandia, I.; Mugica, A.; Zubitur, M.; Arbe, A.; Liu, G.; Wang, D.; Mincheva, R.; Dubois, P.; Müller, A. J. How composition determines the properties of isodimorphic poly (butylene succinate-ran-butylene azelate) random biobased copolymers: from single to double crystalline random copolymers. *Macromolecules* **2014**, 48 (1), 43-57, DOI: 10.1021/ma5023567.

(48) Yu, Y.; Wei, Z.; Liu, Y.; Hua, Z.; Leng, X.; Li, Y. Effect of chain length of comonomeric diols on competition and miscibility of isodimorphism: A comparative study of poly (butylene glutarate-co-butylene azelate) and poly (octylene glutarate-co-octylene azelate). *Eur. Polym. J.* **2018**, 105, 274-285, DOI:10.1016/j.eurpolymj.2018.06.006.

(49) Jeong, Y. G.; Jo, W. H.; Lee, S. C. Cocrystallization behavior of poly (butylene terephthalate-co-butylene 2, 6-naphthalate) random copolymers. *Macromolecules* **2000**, 33 (26), 9705-9711, DOI: 10.1021/ma000040n.

(50) Pérez-Camargo, R. A.; Arandia, I.; Safari, M.; Cavallo, D.; Lotti, N.; Soccio, M.; Müller, A. J. Crystallization of isodimorphic aliphatic random copolyesters: Pseudo-eutectic behavior and double-crystalline materials. *Eur. Polym. J.* **2018**, 101, 233-247, DOI: 10.1016/j.eurpolymj.2018.02.037.

(51) Pan, P.; Inoue, Y. Polymorphism and isomorphism in biodegradable polyesters. *Prog. Polym. Sci*. **2009**, 34 (7), 605-640, DOI: 10.1016/j.progpolymsci.2009.01.003.

(52) Yu, Y.; Wei, Z.; Zhou, C.; Zheng, L.; Leng, X.; Li, Y. Miscibility and competition of cocrystallization behavior of poly (hexamethylene dicarboxylate) s aliphatic copolyesters:

Effect of chain length of aliphatic diacids. *Eur. Polym. J.* **2017**, 92, 71-85, DOI: 10.1016/j.eurpolymj.2017.04.036.

(53) Tan, B.; Bi, S.; Emery, K.; Sobkowicz, M. J. Bio-based poly (butylene succinate-co-hexamethylene succinate) copolyesters with tunable thermal and mechanical properties. *Eur. Polym. J.* **2017**, 86, 162-172, DOI: 0.1016/j.eurpolymj.2016.11.017.

(54) Arandia, I.; Mugica, A.; Zubitur, M.; Arbe, A.; Liu, G.; Wang, D.; Mincheva, R.; Dubois, P.; Müller, A. J. How composition determines the properties of isodimorphic poly (butylene succinate-ran-butylene azelate) random biobased copolymers: from single to double crystalline random copolymers. *Macromolecules* **2015**, 48 (1), 43-57, DOI: 10.1021/ma5023567.

(55) Hong, M.; Tang, X.; Newell, B. S.; Chen, E. Y. "Nonstrained" γ-butyrolactone-based copolyesters: copolymerization characteristics and composition-dependent (thermal, eutectic, cocrystallization, and degradation) properties. *Macromolecules* **2017**, 50 (21), 8469-8479, DOI: 10.1021/acs.macromol.7b02174.

(56) Wang, K.; Jia, Y.-G.; Zhu, X. Two-way reversible shape memory polymers made of cross-linked cocrystallizable random copolymers with tunable actuation temperatures. *Macromolecules* **2017**, 50 (21), 8570-8579, DOI: 10.1021/acs.macromol.7b01815.

(57) Safari, M.; Mugica, A.; Zubitur, M.; Martínez de Ilarduya, A.; Muñoz-Guerra, S.; Müller, A. J. Controlling the Isothermal Crystallization of Isodimorphic PBS-ran-PCL Random Copolymers by Varying Composition and Supercooling. *Polymers* **2020**, 12 (1), 17, DOI: 10.3390/polym12010017.

(58) Safari, M.; Martínez de Ilarduya, A.; Mugica, A.; Zubitur, M.; Muñoz-Guerra, S. n.; Müller, A. J. Tuning the Thermal Properties and Morphology of Isodimorphic Poly [(butylene succinate)-ran-(ε-caprolactone)] Copolyesters by Changing Composition, Molecular Weight, and Thermal History. *Macromolecules* **2018**, 51 (23), 9589-9601, DOI:10.1021/acs.macromol.8b01742.

(59) Socrates, G., *Infrared and Raman characteristic group frequencies: tables and charts*. 3 ed.; John Wiley & Sons: Chichester, UK, 2001.

(60) Partini, M.; Pantani, R. FTIR analysis of hydrolysis in aliphatic polyesters. *Polym. Degrad. Stab.* **2007**, 92 (8), 1491-1497, DOI: 10.1016/j.polymdegradstab.2007.05.009.

(61) Sousa, C.; Leitao, D.; Proenca, M.; Ventura, J.; Pereira, A.; Araujo, J. Nanoporous alumina as templates for multifunctional applications. *Appl. Phys. Rev.* **2014**, 1 (3), 031102, DOI: 10.1063/1.4893546.

(62) Dong, T.; He, Y.; Shin, K. m.; Inoue, Y. Formation and Characterization of Inclusion Complexes of Poly (butylene succinate) with α-and γ-Cyclodextrins. *Macromol. Biosci.* **2004**, 4 (12), 1084-1091, DOI:10.1002/mabi.200400054.

(63) Ciulik, C.; Safari, M.; Martínez de Ilarduya, A.; Morales-Huerta, J. C.; Iturrospe, A.; Arbe, A.; Müller, A. J.; Muñoz-Guerra, S. Poly (butylene succinate-ran-ε-caprolactone) copolyesters: Enzymatic synthesis and crystalline isodimorphic character. *Eur. Polym. J.* **2017**, 95, 795-808, DOI: 10.1016/j.eurpolymj.2017.05.002.

(64) Shi, G.; Liu, G.; Su, C.; Chen, H.; Chen, Y.; Su, Y.; Müller, A. J.; Wang, D. Reexamining the crystallization of poly (ε-caprolactone) and isotactic polypropylene under hard confinement: nucleation and orientation. *Macromolecules* **2017**, 50 (22), 9015-9023, DOI: 10.1021/acs.macromol.7b02284.

(65) Di Lorenzo, M. L.; Androsch, R.; Righetti, M. C. Low-temperature crystallization of poly (butylene succinate). *Eur. Polym. J.* **2017**, 94, 384-391, DOI: 10.1016/j.eurpolymj.2017.07.025.

(66) Chatani, Y.; Okita, Y.; Tadokoro, H.; Yamashita, Y. Structural studies of polyesters. III. Crystal structure of poly-ε-caprolactone. *Polym. J.* **1970**, 1 (5), 555, DOI: 10.1295/polymj.1.555.

(67) Ichikawa, Y.; Kondo, H.; Igarashi, Y.; Noguchi, K.; Okuyama, K.; Washiyama, J. Crystal structures of α and β forms of poly (tetramethylene succinate). *Polymer* **2000**, 41 (12), 4719-4727, DOI: 10.1016/S0032-3861(99)00659-X.